Systems & Control Transactions

Research Article
Foundations of Computer Aided Process Design (FOCAPD 2024)
Breckenridge, Colorado, USA. July 14-18, 2024
Peer Reviewed Conference Proceeding

PSE PRESS

Adsorption-based Atmospheric Water Extraction Process: Kinetic Analysis and Stochastic Optimization

Jinsu Kim[a], Shubham Jamdade[a], Yanhui Yuan[b], and Matthew J. Realff[a]*

[a] Georgia Institute of Technology, Department of Chemical and Biomolecular Engineering, Atlanta, GA, 30332, USA
[b] Avnos, Inc., Los Angeles, CA, 90046, USA
* Corresponding Author: matthew.realff@chbe.gatech.edu.

ABSTRACT

Adsorption-based Atmospheric Water Extraction (AWE) is an energy-efficient distributed freshwater supply method. This research focuses on AWE's kinetic analysis and stochastic optimization, investigating the impact of ambient conditions, kinetics, and weather variability. A one-dimensional fixed-bed system was numerically analyzed using the validated isotherm of MIL-100 (Fe), assuming different kinetic parameters within the linear driving force model. Stochastic optimization, based on annual weather data from Georgia (GA), illustrates the influence of weather conditions on AWE process performance, operation, and cost. Our study offers valuable insights for future research, including site selection, adsorbent material development, and process design. We outline three critical areas for further exploration: experimental verification, material screening, and meteorological site selection.

Keywords: Atmospheric Water Extraction (AWE), Metal-Organic Framework (MOF), Kinetic Analysis, Meteorological Analysis, Two-stage Stochastic Programming (TSSP)

1. INTRODUCTION

Global warming significantly threatens our climate, rendering it increasingly unpredictable. In particular, it changes the natural water cycle, leading to a growing regional freshwater scarcity problem.

The Atmospheric Water Extraction (AWE) process offers a promising solution for sustainable freshwater production(Wang et al., 2022). Among the various AWE techniques, adsorption-based AWE stands out due to its scalability, energy efficiency, and environmental resilience advantages (Xu & Yaghi, 2020).

This study aims to establish a connection between the characteristics of adsorbent materials, kinetic performance, and the variability of weather conditions, contributing to the development of the AWE process from a process systems engineering perspective. In this brief 6-page paper, the AWE process description is very brief; the analysis methods in Sections 2.1 on the S-Shaped Isotherm and Section 2.2 on the Kinetics Analysis are abbreviated, as are many aspects of the process analyses for their temperature and vacuum-swing, adsorption-desorption processes.

2. METHOD

2.1 S-shaped isotherm

MIL-100 (Fe) was selected as the reference MOF material because of its high capacity for moisture uptake (~ 0.75 g_{H2O} g_{ads}^{-1}), and the isotherm model was mathematically formulated in Eqn (1)-(2) by using four isotherm parameters that were previously validated (Kim et al., 2024). $q_{0,max}$ is the theoretical maximum that the MOF can take moisture inside of the structure, K is the distributional factor, which is the function of temperature, and m is the shape factor determining the steepness of the S-shaped isotherm (Sun & Chakraborty, 2014), and h_{evap} is the evaporation heat of moisture.

$$q_{eq} = q_{0,max} \frac{KRH^{m}}{\{1+(K-1)RH^{m}\}} \quad (1)$$

$$K = \alpha \exp\left(\frac{m(Q_{sat,0}-h_{evap})}{RT}\right) \quad (2)$$

2.2 Kinetic analysis

A one-dimensional model of the AWE contactor is proposed in Eqn (3), and a linear-driving force (LDF)

model for the kinetic analysis is defined in Eqn (4). The simulation conditions, including K_{LDF} parameter uncertainty, are shown in **Table 1**.

$$\frac{\partial C_i}{\partial t} + \frac{\partial (uC_i)}{\partial z} + \rho_{ads}(1-\epsilon)\, S = 0 \tag{3}$$

$$S \equiv \frac{dq}{dt} = k_{LDF}(q_{eq} - q) \tag{4}$$

Table 1: Simulation conditions for the numerical analysis.

Physical dimension	**Value**
Length (L)	200 mm
Area (A)	0.5 m^2
Charged mass	2.91 kg_{MOF}/m^3_{Bed}
Ambient conditions	
Air velocity (u)	1.0 m/s
Temperature (T)	0, 10, 20, 30 °C
Humidity (RH)	20, 40, 60, 80 %
Kinetic parameter	
k_{LDF}	0.5, 0.05, 0.005, 0.005 1/s

2.3 Key Performance Indicators

For the intrinsic performance measures of the AWE process, the average bed utilization was analyzed in Eqn (5). From an economic perspective, we introduced the cost of moisture capture (CoMC) as an objective function for stochastic programming. The detailed formulation of cost and energy was taken from the previous work (Kim et al., 2024).

$$Bed_{util}(\%) = \frac{q}{q_{eq}} \times 100 \tag{5}$$

$$CoMC\ \left(¢\ kg^{-1}_{H_2O}\right) = \frac{\text{Annualized capital+operating}}{\text{The total captured moisture}} \tag{6}$$

2.4 Two-stage stochastic programming

Two-stage stochastic programming (TSSP) was developed to address the variability of ambient weather conditions and ensure the operability of the process.

To solve the 1st stage, a grid search was performed over a sufficiently wide range of capital costs. A conservative weather condition was selected to decide the upper bound on capital cost. Capital cost was evenly gridded out in the range of +/-20% of base cost as shown in Eqn (7). After defining the grid, the minimization problem in the 2nd stage was iteratively solved in Eqn (8). The binary decision variables represented whether or not to operate at a given weather condition. The i^{th} objective function was the sum of the i^{th} annualized capital cost and the expectation of the operating cost divided by the expectation of the harvesting performance. Here, the operating cost and the swing capacity were the functions of capital cost, C_i.

The more capital invested the better the performance in specific weather scenarios but with reduced effectiveness as the capital investment increases further. The performance decreases at lower capital and eventually this reduced performance increases the overall average cost. The minimum of the overall cost was located within the grid search for all examples we have studied. Should it appear at the extreme of a range a further expansion of the grid should be performed.

By separating the decision-making process from weather uncertainties within the two-stage framework, we achieved scalable solutions for screening potential MOF candidates and identifying a favorable site.

$$C_i = Grid\ of\ [0.8\min(C_{cons}), 1.2\max(C_{cons}), 8] \tag{7}$$

$$minimize\ Obj_i = \frac{C_i \times f_{an} + \mathrm{E}[B^{\mathrm{T}} OPEX(C_i)]}{\mathrm{E}[B^{\mathrm{T}} \mathrm{q}_{\mathrm{swing}}(C_i)]} \tag{8}$$

3. RESULTS AND DISCUSSION

3.1 Numerical code verification

The original PDE was semi-discretized and then numerically analyzed in MATLAB using an ode15s solver. The simulation results are consistent with those simulated by the commercial software (Oh et al., 2020), gPROMS, and the relative numerical error of the mass balance in Eqn (9)-(11) was under 0.05%.

$$m_1 = \mathrm{Au} \int_0^t (C_{init} - C_{exit})\, dt \tag{9}$$

$$m_2 = (1-\varepsilon_{bed})(1-\varepsilon_s)\rho_s \mathrm{AL} \frac{10^3}{18} \int_0^Z q\, dz \tag{10}$$

$$Err_{rel} = 100 \times \frac{|m_1 - m_2|}{m_1} \tag{11}$$

The following section illustrates the impacts of ambient conditions and hypothetical kinetic parameters. Finally, we provide TSSP results for the example of the state of Georgia, USA, using weather data.

3.2 Saturation time

Saturation time gives direct information for the process design and operation variables such as the dimension of the bed, adsorption time, and required amount of MOF, etc. We showed how the saturation time changes alongside the value of absolute humidity, as shown in **Fig. 1**, by simplifying that the value is relatively unchanged during the diurnal cycle.

This fluctuation implied that the operating variable, adsorption time should be adaptively designed considering the ambient condition. Each variable was parametrically studied, focusing on the breakthrough behavior and bed saturation as follows.

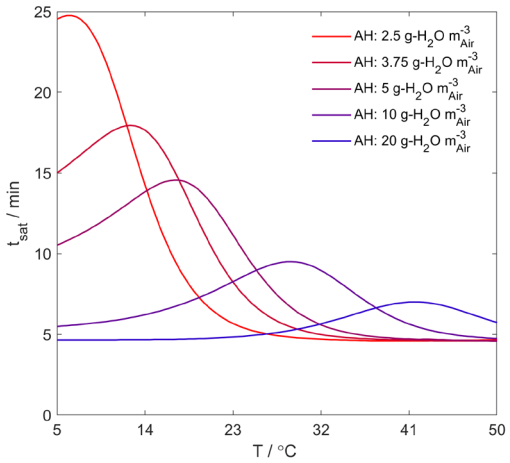

Figure 1: Saturation time variation according to the level of absolute humidity.

3.3 Effects of ambient temperature

The ambient temperature directly affects the bed utilization ratio, and the high-temperature conditions enable the bed to reach a faster saturation state, as shown in **Fig. 2a**. This was determined by the concentration difference given the fixed kinetic parameter in every condition. In **Fig. 2b**, the normalized exit concentration profiles showed that breakthrough occurred slower in the low-temperature condition, consistent with **Fig. 2a**. The experiments on temperature sensitivity should be supported to support the simulation results, which should be the future work.

3.4 Effects of ambient humidity

The effects of relative humidity are shown in **Fig. 3** by fixing the ambient temperature. The RH and the bed utilization were not directly related, as shown in **Fig. 3a**. Firstly, q_{eq} increased as RH increased following the S-shape. Secondly, the moisture concentration increased as RH increased linearly. These two compensated each other, causing a minimal impact on performance. Although the bed saturation behavior showed similar results, the absolute amount of moisture and the regenerability directly affect the performance, which should be discussed further. As seen in **Fig. 3b**, RH had apparent effects on breakthrough behavior. Because of the low concentration and the low q_{eq}, the driving force of moisture capture was low in low-temperature conditions.

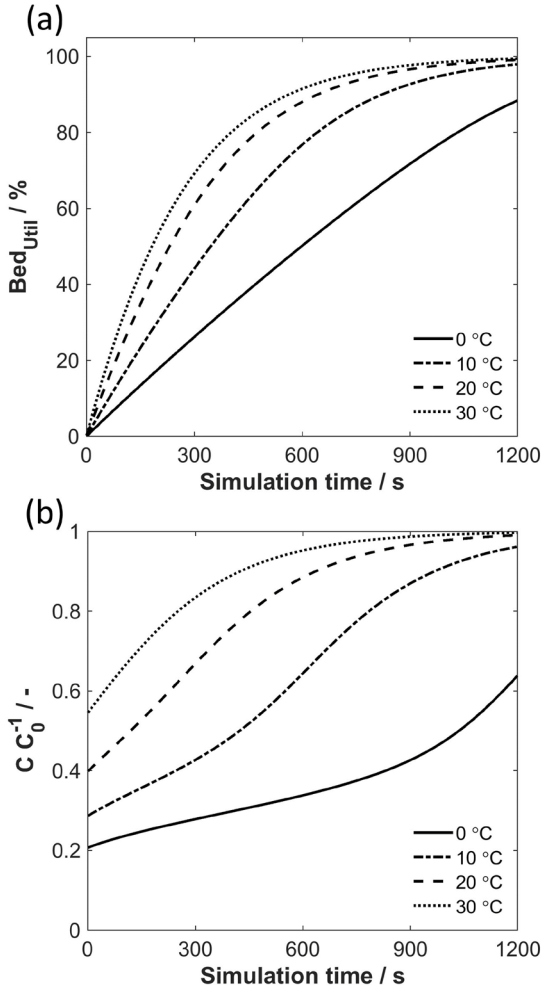

Figure 2: The effects of ambient temperature on (a) bed utilization ratio and (b) breakthrough curve on normalized moisture concentration at RH 50% condition (k_{LDF} assumed as 0.005 s^{-1}).

3.5 Effects of kinetic parameter

Finally, the sensitivity of the hypothetical kinetic parameters was analyzed in **Fig. 4**. By taking the ranges of LDF parameters reported in the literature, the expected profiles on the bed utilization and the breakthrough were predicted. Regarding bed utilization, the impact of the kinetic parameters was asymmetric in **Fig. 4a**. As the kinetic parameters became smaller, utilization decreased monotonically. However, the utilization curve converged when the kinetic parameters became more prominent. It failed to observe the breakthrough curve in the slowest case, and the breakthrough behavior in the fastest case was observed in **Fig. 4b**.

For the stochastic optimization, we fixed the k_{LDF} as 0.005 s^{-1}, taken from the moisture uptake systems over Silica gel (El-Sharkawy, 2011).

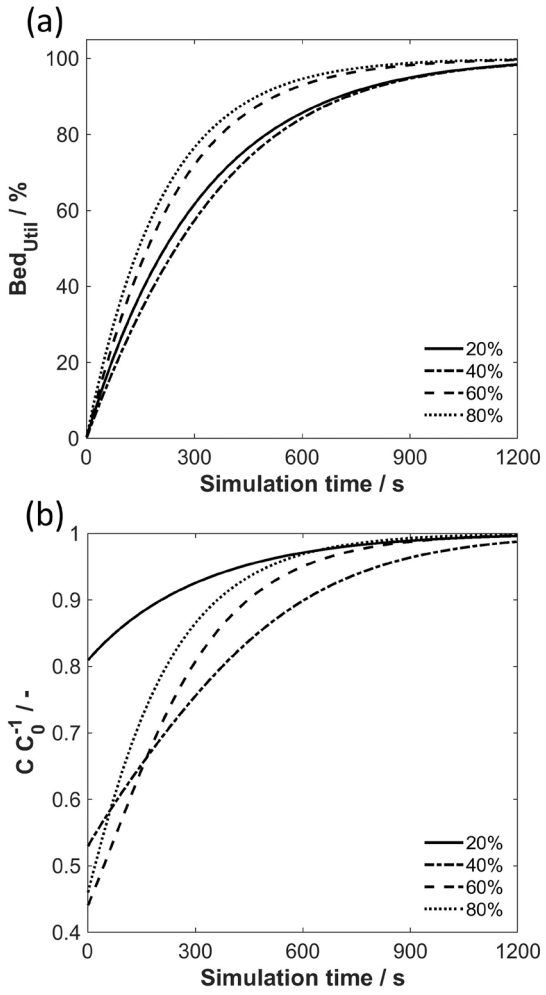

Figure 3: The effects of ambient relative humidity on (a) bed utilization ratio and (b) breakthrough curve on normalized moisture concentration at temperature 25°C condition (k_{LDF} assumed as 0.005 s^{-1}).

3.6 Optimization results

The original weather data was plotted as a function of temperature and RH. The data source originated from the Automated Surface Observing Systems (ASOS) of daily measurements during 2022. In **Fig. 5**, probability distribution was plotted, and the 100 random samples were marked in '**x**,' representing the original distribution well. The source and sampling algorithm was provided in previous work (Kim et al., 2024). Stochastic optimization was conducted utilizing the random samples.

Fig. 6a shows stochastic optimization results by dividing the economically feasible and infeasible regions from the programming algorithm. It was observed that the feasible region was clustered in the mild RH range (>40 %) and mild temperature range (2~25℃). **Fig. 6b** shows how the capital cost was selected in the design grid. The programming results were repeated three times, and the average and standard deviation were plotted to consider the randomness of the sampling. The 5th grid point was selected for the first-stage decision because it balanced capital against performance and hence achieved the minimum cost without sacrificing the swing capacity. These results showed the tailored optimal solution based on selecting the optimal capital investment, operating degrees of freedom and conditions in which to operate simultaneously.

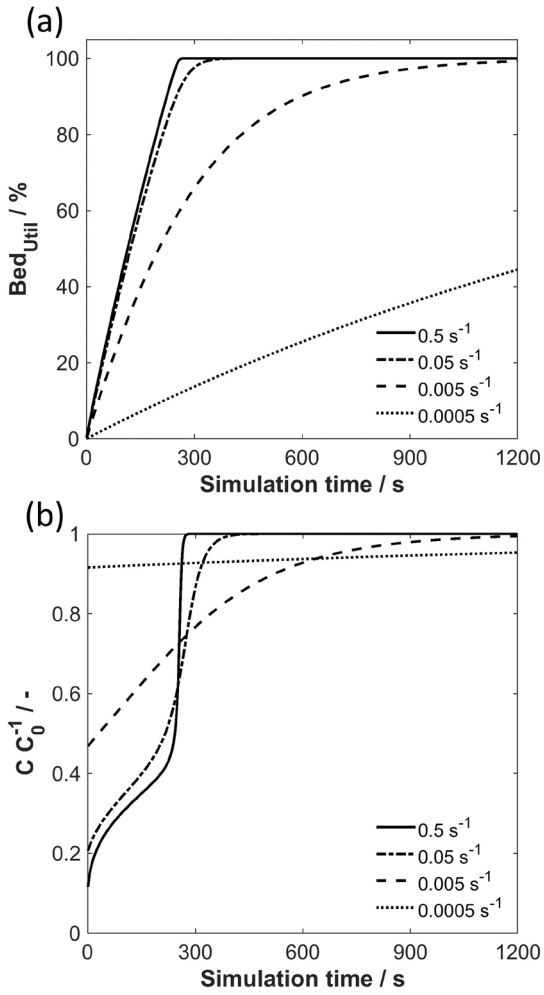

Figure 4: The effects of kinetic parameter on (a) bed utilization ratio and (b) breakthrough curve on normalized moisture concentration at temperature 25°C and RH 50% condition.

Fig. 7 demonstrates the relationship between performance and cost. The color shows the economic feasibility, red or blue, for infeasible and feasible respectively. Blue has an average performance of 0.67 kg_{H2O} kg_{Ads}^{-1} with 4.04 ¢ kg_{H2O}^{-1}. Red has a performance of 0.36 kg_{H2O} kg_{Ads}^{-1} with 5.38 ¢ kg_{H2O}^{-1}.

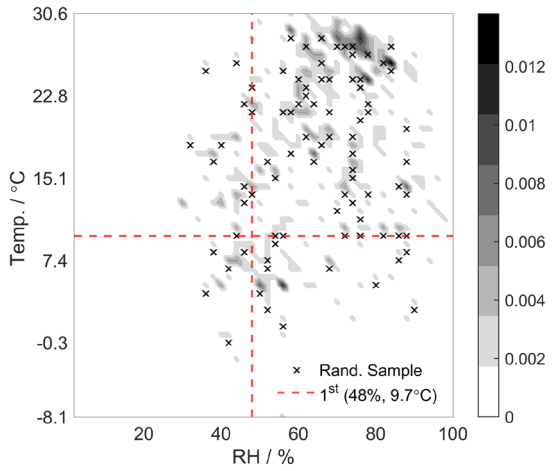

Figure 5: Weather variability as a joint probability function for Georgia, USA, and random sampling (n= 100) for the stochastic optimization.

3.7 Future work

Three areas should be expanded on to better understand the adsorption-based AWE process. First, experiments are required to refine the kinetic parameter value from the hypothetical range given here. Different temperature and RH conditions should be experimentally measured together for rigorous validation. Second, different types of material should be compared to derive the main factors that influence design and operation, including isotherm shape and moisture uptake. Molecular simulation will be appropriate for the massive screening (Zhang et al., 2023). Lastly, various meteorological sites could be investigated further, including varying the operation based on the time of day.

4. CONCLUSION

Based on the critical issues summarized herein, the AWE process is promising for producing fresh water. Process design and weather uncertainties are discussed together, starting from the isotherm features at the material level. This work aims to bridge the gap between material and process development to realize robust design and operation. It directs the future research of adsorption-based AWE systems in perspectives on process systems engineering. From this initial work, a generalized framework for simultaneous material-process selection in different climates accounting for weather variability can be developed in the future.

Through this work, we contribute to two areas (i) understanding the system's dynamics and (ii) quantifying the meteorological characteristics, thereby giving insights into process systems engineering (PSE) aspects of the AWE process.

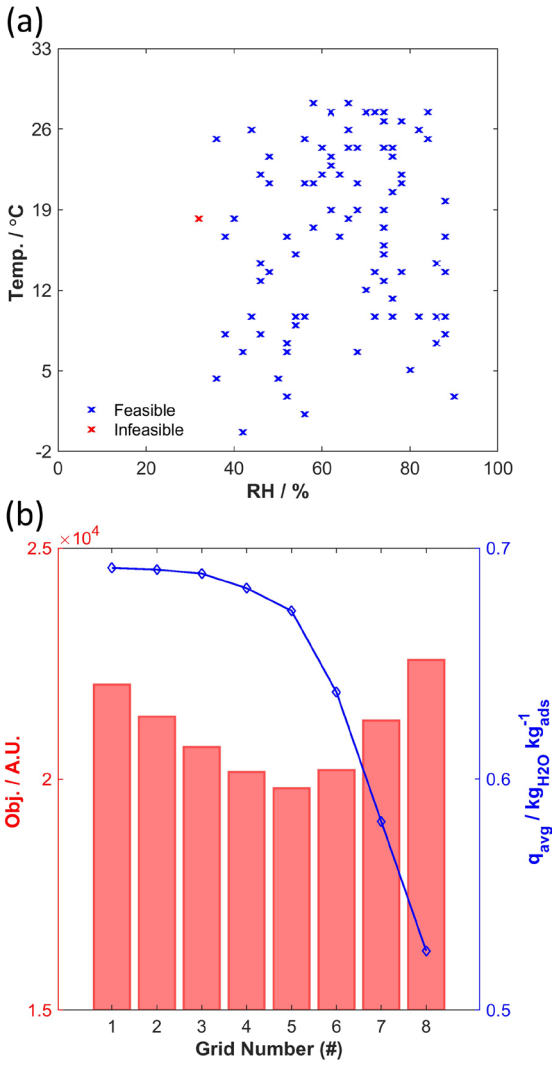

Figure 6: Two-stage stochastic programming results for (a) the identification of the feasible weather conditions and (b) the decision of conservative capital cost from average swing capacity.

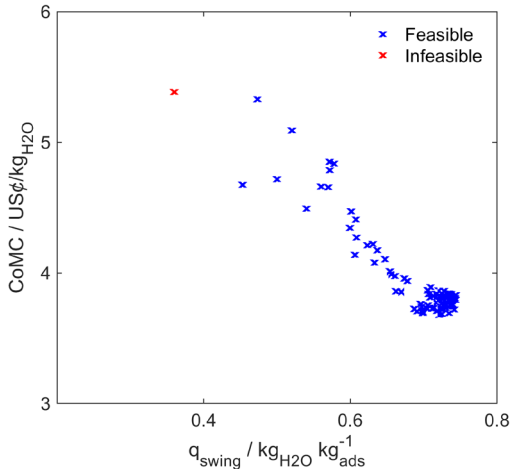

Figure 7: The relationship between water extraction performance and cost of moisture capture according to the weather feasibility in terms of economics.

ACKNOWLEDGEMENTS

Jinsu Kim was supported by a sub-award to Georgia Tech from ONR N00014-23-C-1011. Any opinions, findings, conclusions, or recommendations expressed in this material are those of the author(s) and do not necessarily reflect the views of the Office of Naval Research.

REFERENCES

1. El-Sharkawy, I. I. (2011). On the linear driving force approximation for adsorption cooling applications. *International Journal of Refrigeration*, *34*(3), 667–673.
2. Kim, J., Jamdade, S., Yuan, Y., & Realff, M. J. (2024). System-level analysis of atmospheric water extraction with MIL-100 (Fe) for design and optimal site selection using meteorological characteristics. *Energy*, *299*, 131376.
3. Oh, H., Beum, H. T., Yoon, Y.-S., Kim, J., Han, Y., Kim, J., Lee, I.-B., Lee, S.-Y., & Han, S. S. (2020). Experiment and Modeling of Adsorption of CO from Blast Furnace Gas onto CuCl/Boehmite. *Industrial & Engineering Chemistry Research*, *59*(26), 12176–12185. https://doi.org/10.1021/acs.iecr.0c01752
4. Sun, B., & Chakraborty, A. (2014). Thermodynamic formalism of water uptakes on solid porous adsorbents for adsorption cooling applications. *Applied Physics Letters*, *104*(20), 201901.
5. Wang, J., Hua, L., Li, C., & Wang, R. (2022). Atmospheric water harvesting: Critical metrics and challenges. *Energy & Environmental Science*, *15*(12), 4867–4871.
6. Xu, W., & Yaghi, O. M. (2020). Metal–organic frameworks for water harvesting from air, anywhere, anytime. *ACS Central Science*, *6*(8), 1348–1354.

© 2024 by the authors. Licensed to PSEcommunity.org and PSE Press. This is an open access article under the creative commons CC-BY-SA licensing terms. Credit must be given to creator and adaptations must be shared under the same terms. See https://creativecommons.org/licenses/by-sa/4.0/